Road Surface Condition Monitoring Using Fully Polarimetric Airborne SAR Data

Arun Babu[a], Stefan V. Baumgartner[a] and Gerhard Krieger[a]
[a] Microwaves and Radar Institute, German Aerospace Center (DLR), Wessling, Germany
Email: arun.babu@dlr.de

Abstract

Since the proper maintenance of the road infrastructure has a crucial role in economic development and also on the people's safety, the periodic monitoring of the road surface quality is a necessity. The widely used method of road surface condition monitoring using measurement vehicles all over the country is costly, labour intensive and time-consuming. The potential of fully polarimetric airborne SAR to remotely monitor the road surface roughness, cracks and potholes are investigated in this study using fully polarimetric X-band SAR datasets acquired with DLR's F-SAR airborne SAR system. The former military airfield at Kaufbeuren is selected as the test site for this study. The polarimetric analysis revealed that the anisotropy and coherency matrix ($T3$) elements are sensitive to the road surface roughness and can be used to retrieve the vertical surface roughness. Also, the SAR backscatter based empirical models are found to be sensitive to the road surface roughness variations. The cross-polar sigma nought images show a considerable increase in their magnitude over the cracks and potholes on the road surface. The initial experimental results obtained from this study are discussed in this paper.

1 Introduction

The road network has a major influence on the development of a country and the problems associated with the traffic network have a direct negative impact on the Gross Domestic Product (GDP) of the country. Also, the quality of the road network is very important for the safety, health and driving comfort [1]. The road surface roughness, cracks and potholes are important factors which affect the road surface quality. The cracks and potholes occur annually due to the freeze-thaw cycles during the winter season [2]. The cracks and potholes cause damage to the vehicles, lead to accidents, increase maintenance costs and reduce the lifetime of the vehicles. Road surface roughness influences the 'skid resistance' of the vehicle [3]. Sufficient amount of skid resistance is required for performing safe acceleration, deceleration and steering manoeuvres. Several studies have proven that poor skid resistance leads to a higher accident probability [4].
Because of all the above-mentioned factors, the periodic monitoring of the road network is necessary to keep track of the changes in its present condition. For instance, in Germany the road surface condition is measured once in every four years which may not be sufficient in some cases. So far, the measurement is carried out manually using measurement vehicles. This requires enormous costs for the entire road network because of its labour intensive and time-consuming nature [5].
This study focuses on evaluating the potential of polarimetric airborne SAR to remotely estimate the road surface conditions on a large scale. So far, not much literature for road surface roughness estimation is available. The prime objective of this study is to investigate and develop efficient and reliable methods for road surface roughness estimation and also for the detection of cracks and potholes. In the near future, the continuous road condition monitoring can help in the refinement of the digital traffic infrastructure maps which can provide the user with prior knowledge of the road conditions.

2 Study Area and Dataset

2.1 Study Area

The Kaufbeuren test site located in Bavaria, Germany is considered for this study (**Figure 1**). It is a former military airfield that includes the runway, taxiways and parking areas composed of different materials (e.g., asphalt, concrete) and, thus, have different surface roughness, also cracks and potholes are present there (see zoomed view inside the red rectangle in **Figure 1**).

Figure 1 Kaufbeuren test site showing a zoomed view of the cracked parking area

All these factors make this test site a perfect candidate for this study.

2.2 Dataset

Table 1 Metadata of the F-SAR dataset

Parameters	Value
Date of acquisition	22.10.2018
Polarization	Quad-pol
Centre frequency	9.6 GHz
Range resolution	0.25 m
Azimuth resolution	0.25 m

The fully polarimetric X-band dataset acquired with DLR's airborne F-SAR sensor over the Kaufbeuren test site is used for this study. The details about the dataset are shown in **Table 1**.

3 Methodology

The flow chart of the methodology adopted for the road surface roughness estimation and the detection of cracks and potholes is shown in **Figure 2**.

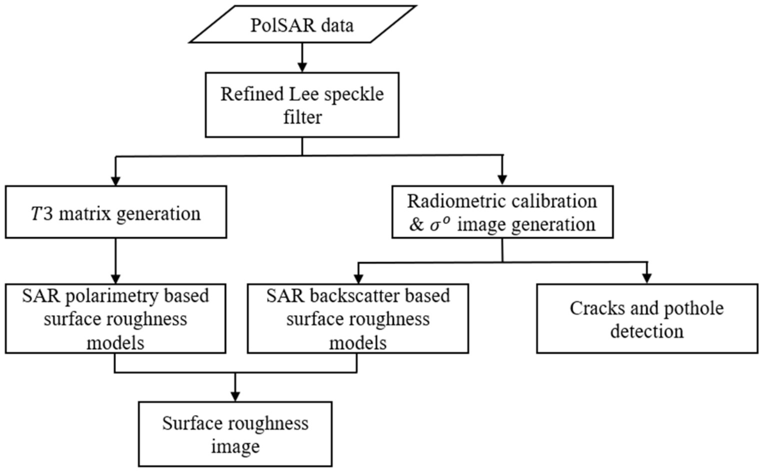

Figure 2 Methodology flowchart

3.1 Road surface roughness estimation

The dataset is first speckle filtered using a 3x3 refined-Lee speckle filter. In this study, two SAR polarimetry and three SAR backscatter-based surface roughness models were implemented to estimate the surface roughness of the roads.

3.1.1 SAR polarimetry based approach

The fully polarimetric SAR dataset can be represented in the form of the Pauli basis vector (k_p) as follows [6]:

$$k_p = \frac{1}{\sqrt{2}}\begin{pmatrix} S_{HH} + S_{VV} \\ S_{HH} - S_{VV} \\ 2S_{HV} \end{pmatrix}. \tag{1}$$

The 3x3 polarimetric coherency matrix ($T3$) can be generated by multiplying the Pauli basis vector (k_p) with the transpose of its complex conjugate (k_p^{*T}):

$$T3 = \langle k_p \, . \, k_p^{*T} \rangle \tag{2}$$

where $\langle ... \rangle$ indicates spatial ensemble averaging.

From the PolSAR data, the remotely sensed parameter (ks), which represents the effective vertical roughness, can be derived. In this study, the polarimetric scattering anisotropy generated from the eigenvalues of the coherency matrix $T3$ and the elements of the $T3$ matrix itself are considered to generate the ks parameter.

According to the eigendecomposition theorem, the 3x3 coherency matrix $T3$ can be represented as follows [7]:

$$T3 = [U_3][\Sigma_3][U_3]^{*\mathrm{T}}. \tag{3}$$

The 3x3 real, diagonal matrix $[\Sigma_3]$ contains the eigenvalues of $T3$ [8]:

$$[\Sigma_3] = \begin{bmatrix} \lambda_1 & 0 & 0 \\ 0 & \lambda_2 & 0 \\ 0 & 0 & \lambda_3 \end{bmatrix} \tag{4}$$

where $\lambda_1 \geq \lambda_2 \geq \lambda_3 \geq 0$.

The anisotropy parameter (A) is generated as follows [8]–[10]:

$$A = \frac{\lambda_2 - \lambda_3}{\lambda_2 + \lambda_3}. \tag{5}$$

The effective vertical roughness ks can be estimated from the anisotropy parameter as follows [11], [12]:

$$ks = 1 - A. \tag{6}$$

So, ks estimated using the anisotropy parameter is based on the 2nd and 3rd eigenvalues of the coherency matrix.

As an alternative, the vertical roughness ks can also be estimated directly from the T_{22} and T_{33} elements of the coherency matrix [9], [12]:

$$ks = 1 - \frac{T_{22} - T_{33}}{T_{22} + T_{33}}. \tag{7}$$

3.1.2 SAR backscatter based approach

The Oh models developed in 1992 [13], 2004 [14] and the Dubois model developed in 1995 [15] for surface roughness and soil moisture estimation are considered here. These models were originally developed for bare soil and agricultural fields. The usability of these models for the surface roughness estimation of an asphalt road is evaluated in this study.

The inversion of the Oh model 1992 is based on solving the following non-linear equation using a root solving algorithm:

$$\left(\frac{2\theta}{\pi}\right)^{\frac{1}{\Gamma^o}}\left[1 - \frac{q}{0.23\sqrt{\Gamma^o}}\right] + \sqrt{p} - 1 = 0. \tag{8}$$

The above non-linear equation needs to be solved iteratively to estimate the Fresnel reflectivity of the surface at nadir (Γ^o). The parameter θ is the incidence angle, p is the co-polarized ratio and q is the cross-polarized ratio. The ks can be estimated from the Γ^o as follows:

$$ks = \ln\left(\frac{\left(\sqrt{p} + 1\right)}{\left(\frac{2\theta}{\pi}\right)^{\frac{1}{3\Gamma^o}}}\right). \tag{9}$$

The inversion of ks using the Dubois model is a two-step non-iterative process. The 1st step is to estimate the dielectric constant (ε') as follows:

$$\varepsilon' = \frac{\left(\log 10\left(\frac{(\sigma_{HH}^o)^{0.7857}}{\sigma_{VV}^o}\right) 10^{-0.19} \cos^{1.82}\theta \, \sin^{0.93}\theta \, \lambda^{0.15}\right)}{-0.024 \tan\theta} \tag{10}$$

where σ_{HH}^0 and σ_{VV}^0 are the co-polar sigma nought values for HH and VV channels, respectively. The 2nd step is to derive ks from the estimated dielectric constant (ε') as follows:

$$ks = {\sigma_{HH}^{o}}^{1/1.4} 10^{2.75/1.4} \frac{\sin^{2.57}\theta}{\cos^{1.07}\theta} 10^{-0.02\varepsilon' \tan\theta} \lambda^{-0.5}. \tag{11}$$

In the Oh model 2004, the surface moisture (mv) is estimated to derive ks in contrast to the Oh model 1992. The surface moisture (mv) is estimated by solving the following non-linear equation using an iterative root-finding algorithm:

$$1-\left(\frac{\theta}{90}\right)^{0.35mv^{-0.65}} e^{-0.65}\left[\left[-3.125\ln\left\{1-\frac{\sigma_{VH}^{o}}{0.11mv^{0.7}\cos^{2.2}\theta}\right\}\right]^{0.556}\right]^{1.4} - p = 0. \tag{12}$$

Then ks is estimated as follows:

$$ks = \left[-3.125\ln\left\{1-\frac{\sigma_{VH}^{o}}{0.11mv^{0.7}\cos^{2.2}\theta}\right\}\right]^{0.556}. \tag{13}$$

The Root Mean Square (RMS) height (h_{rms}), which is the RMS average of the vertical profile heights of a surface, is used for the vertical surface roughness characterization and can be derived from ks using the following equation [11]:

$$h_{rms} = \frac{ks}{(2\pi/\lambda_c)} \tag{14}$$

where λ_c is the centre frequency of the SAR system.

The ks values estimated from the Oh models have a validity range of $0.1 < ks < 6.0$ [13], [14]. This corresponds to a h_{rms} validity range of 0.49 mm $< h_{rms} <$ 29.82 mm for an X-band sensor with 9.60 GHz frequency. For the Dubois model, the measured ks values are valid when $ks < 2.5$ and the incidence angle $(\theta) > 30^o$ [15]. This corresponds to a h_{rms} validity range of $h_{rms} <$ 12.43 mm for an X-band sensor with 9.60 GHz frequency.

3.2 Cracks and pothole detection

The radiometrically calibrated sigma nought (σ^0) images of the four polarization channels are analysed to investigate the effects of cracks and potholes in the co-polarized and cross-polarized channels. The sigma nought (σ^0) images are calculated as follows [16]:

$$\sigma_{dB}^0 = 10 \cdot \log_{10}(|I|^2 \sin\theta_{inc.}) \tag{15}$$

where θ_{inc} is the local incidence angle and I is the single-look complex (SLC) image of the respective channel.

4 Preliminary Experimental Result

This study was started in September 2019 and the initial results of the road surface roughness, cracks and potholes estimated using the techniques described in the previous section are discussed here.

4.1 Road Surface Roughness

Figure 3 shows the intensity HH image of the test site.

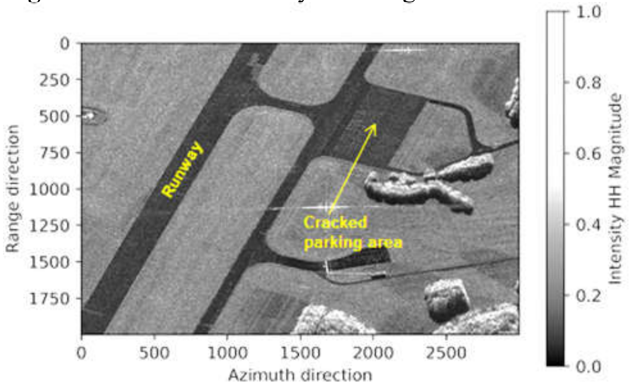

Figure 3 Intensity HH image of the Kaufbeuren test site

The Kaufbeuren runway and the cracked parking area can be seen in the image.

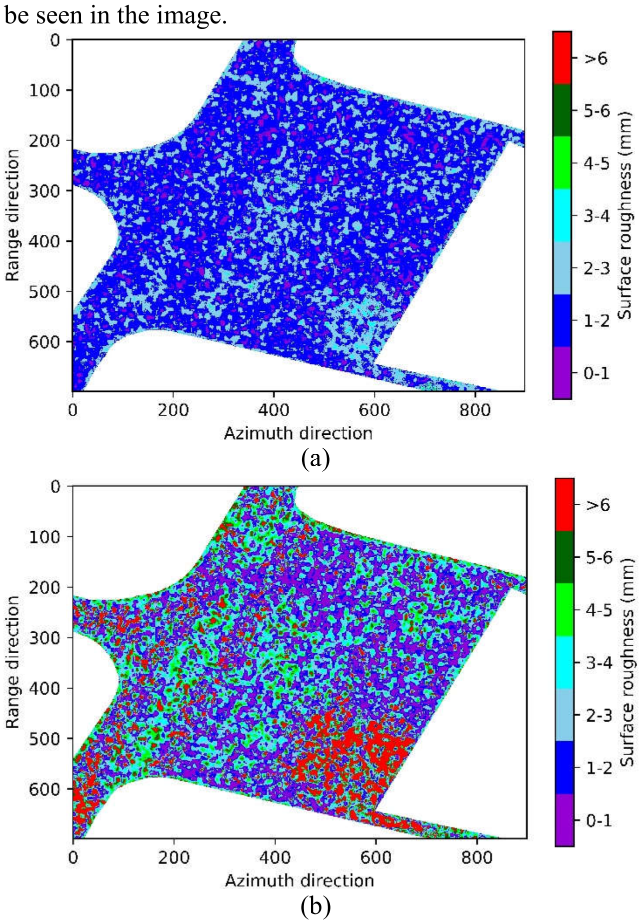

Figure 4 h_{rms} images; **(a)** from anisotropy; **(b)** from T3 matrix.

Figure 4 (a) shows the h_{rms} image of the cracked parking area estimated from the anisotropy parameter. By comparing this image with the Google Earth image of the cracked parking area shown in **Figure 1**, it can be seen that there is a noticeable increase in the surface roughness at the cracked regions. But since the anisotropy parameter is estimated from the minor eigenvalues (2nd and 3rd) of the $T3$ matrix, the h_{rms} image appears to be noisy. **Figure 4 (b)** shows the h_{rms} image generated from the $T3$ matrix elements. A similar trend in roughness variation can be observed in both figures. But **Figure 4 (b)** shows higher values of roughness for the same areas in **Figure 4 (a)**.

The severely cracked road areas can be better differentiated in **Figure 4 (b)** compared to **Figure 4 (a)**.

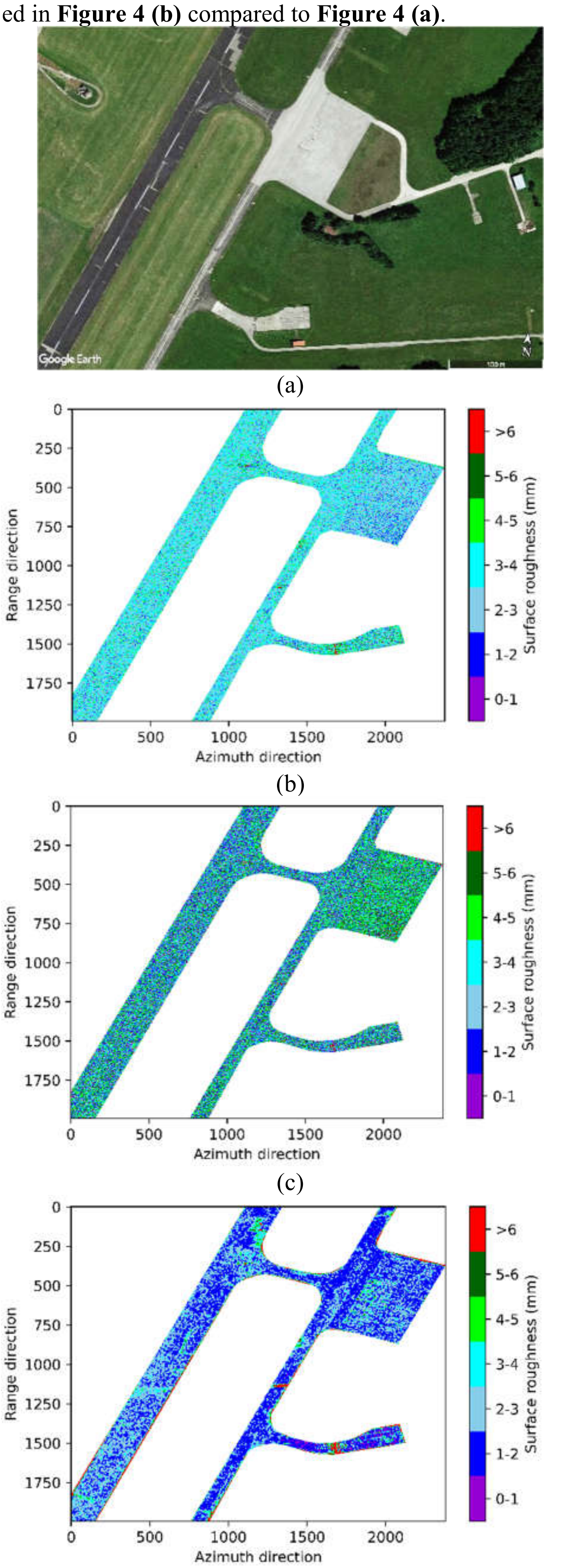

Figure 5 (a) Google Earth image; **(b)** h_{rms} image from Oh 1992 model; **(c)** h_{rms} image from Oh 2004 model; **(d)** h_{rms} image from Dubois model

Figure 5 (a) shows the zoomed Google Earth image of the Kaufbeuren runway and the cracked parking area. Figure 5 (b) and Figure 5 (c) shows the h_{rms} images estimated using the Oh 1992 and Oh 2004 models, respectively. By comparing both images with the Google Earth image, it can be seen that both images appear to be noisy and the change in road surface roughness between the cracked and non-cracked regions cannot be well distinguished. Figure 5 (d) shows the h_{rms} image estimated from the Dubois model. By analysing and comparing this image with the Google Earth image it can be found that the difference in surface roughness between the concrete and asphalt regions are visible in the h_{rms} image. Also, the cracked regions at the parking area are showing a higher value of h_{rms} compared to the surrounding smooth regions.

4.2 Cracks and Potholes

The effect of cracks and potholes on the co-polar and cross-polar sigma nought images are discussed here.

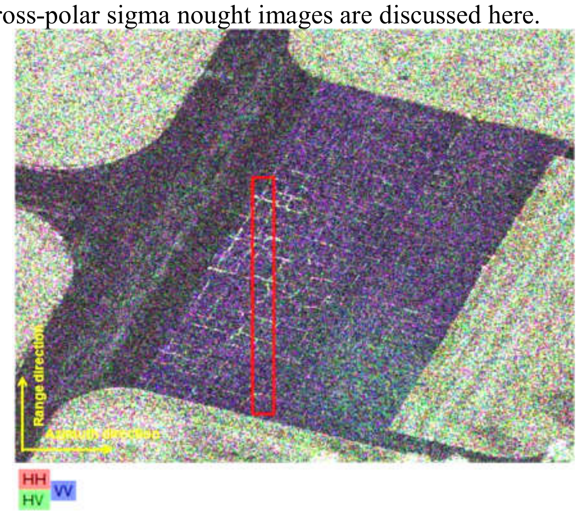

Figure 6 RGB composite generated from F-SAR intensity images.

Figure 6 shows the RGB composite of the intensity images with HH channel as the red band, HV channel as the green band and VV channel as the blue band. The cracks can be seen in the image and the severely cracked road region inside the red rectangle is chosen to analyse the effect of cracks on co-pol and cross-pol channels.

Figure 7 (a) and **(b)** shows the co-polar sigma nought images generated from the HH and VV channels, respectively. By comparing **Figure 7 (a)** with the Google Earth image shown in **Figure 1**, it can be seen that even though some of the severe cracks are visible in the sigma nought HH image, the other cracks, potholes and their patterns cannot be identified. The same is valid for the sigma nought VV image (**Figure 7 (b)**). However, the sigma nought values may depend on the aspect angle or direction of the cracks so that by looking to the preliminary results obtained from a single data set no conclusions regarding the usability of HH and VV can be drawn.

The cross-polar sigma nought images generated from the HV and VH channels are shown in **Figure 7 (c)** and **(d)**, respectively. By comparing both **Figures 7 (c)** and **(d)** with the Google Earth image of the cracked road area (**Figure 1**), it can be seen that most of the cracks, potholes and their patterns are visible in the sigma nought HV and VH images.

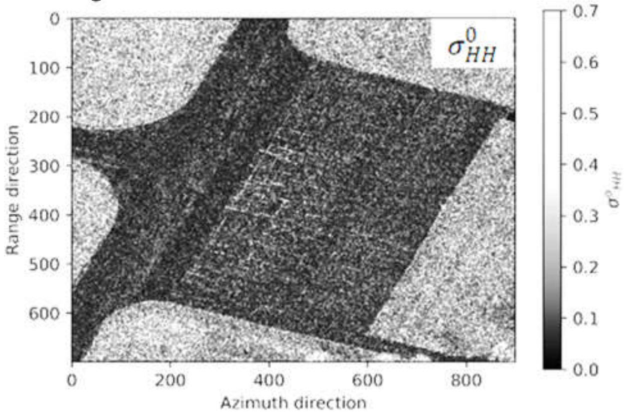

(a)

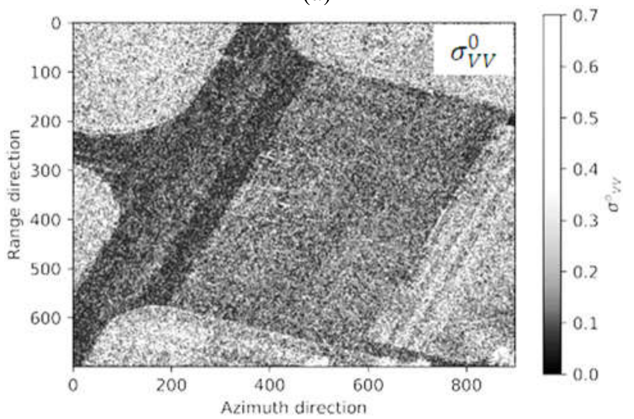

(b)

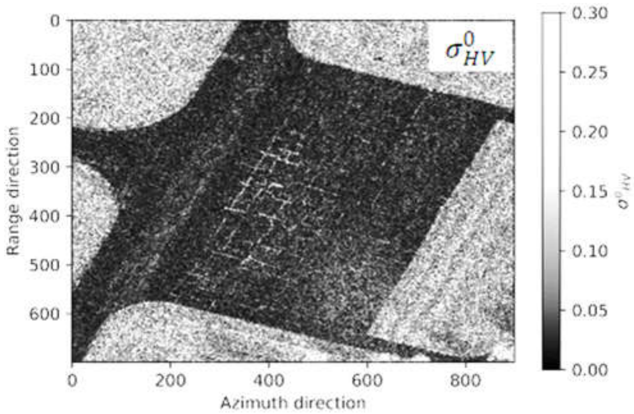

(c)

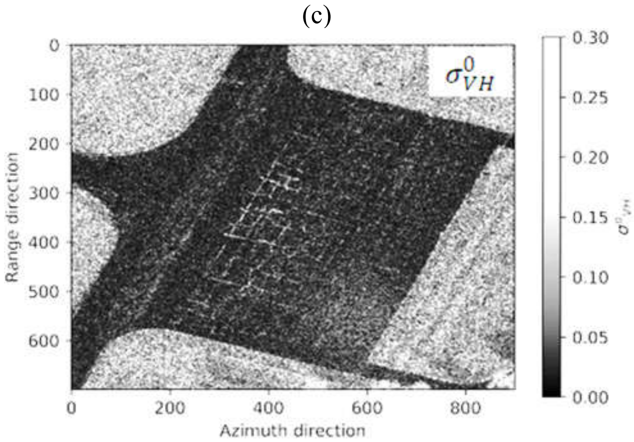

(d)

Figure 7 Sigma nought (σ^0) images.

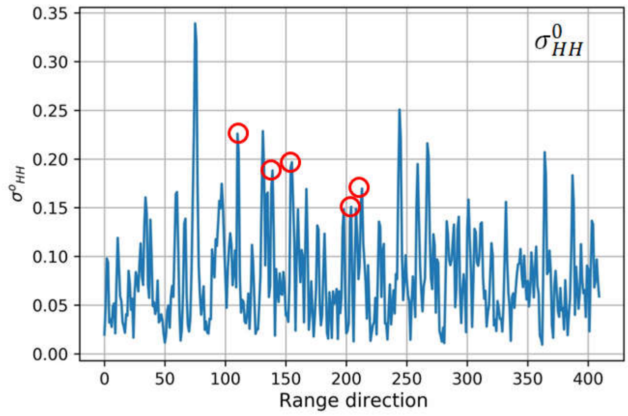

(a)

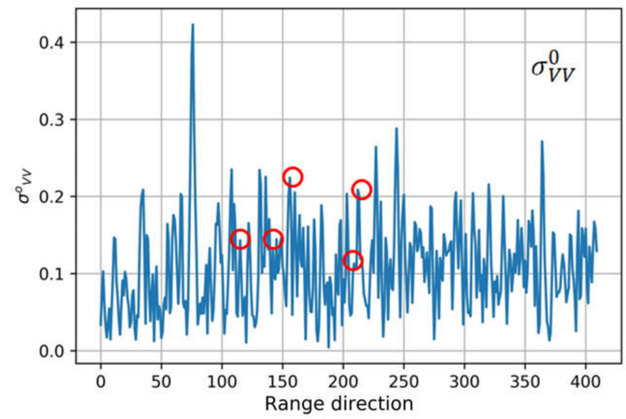

(b)

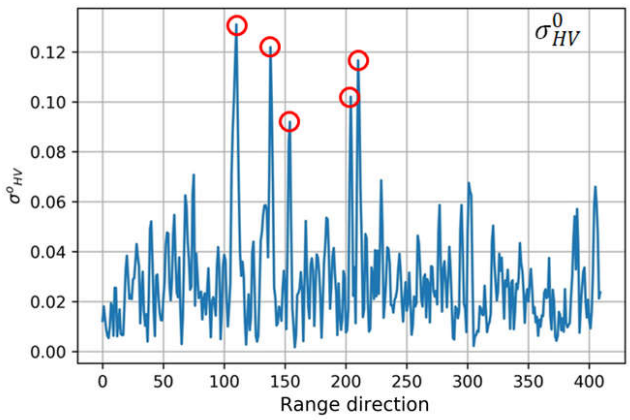

(c)

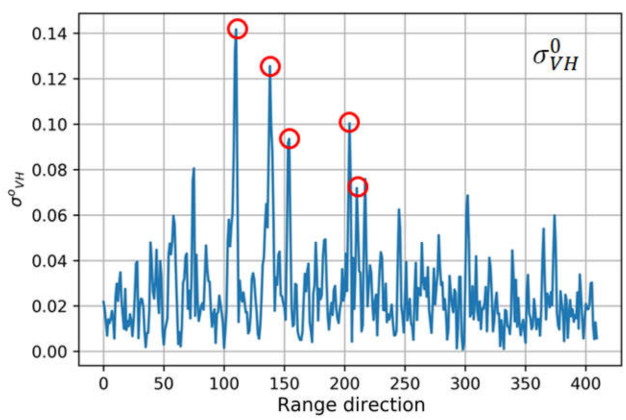

(d)

Figure 8 Sigma nought (σ^0) magnitude plots.

Figure 8 (a) and **(b)** shows the magnitude plots for the co-polar sigma nought HH and VV channels (σ_{HH}^{0} and σ_{VV}^{0}), respectively, and the expected crack positions are indicated by the red circles. The plots are generated from the severely cracked road section along the range direction shown inside the red rectangle in **Figure 6**. By analysing the sigma nought HH (σ_{HH}^{0}) magnitude plot it can be seen that there is only a small increase in the order of 0.05 to 0.08 in the cracked road areas compared to the surrounding smooth road sections. The sigma nought VV (σ_{VV}^{0}) magnitude plot (**Figure 8 (b)**) shows that there is a negligible influence of the cracks and potholes on the sigma nought VV (σ_{VV}^{0}) magnitude.

Figure 8 (c) and **(d)** shows the magnitude plots for the cross-polar sigma nought HV and VH (σ_{HV}^{0} & σ_{VH}^{0}) channels, respectively. By analysing both magnitude plots at the cracked positions on the road indicated by red circles, it can be seen that there is a relative increase of magnitude up to approximately 0.13 at the severely cracked road regions compared to the surrounding smooth regions.

5 Conclusion

Polarimetric SAR data are sensitive to road surface roughness and thus show great potential for wide-area road surface condition monitoring. The anisotropy and $T3$ matrix elements are showing a variation in h_{rms} between smooth and cracked road regions. The empirical models developed for the surface roughness and soil moisture estimation of bare soils and agricultural lands have the potential to estimate the millimetre level surface roughness of smooth road surfaces. Out of all the models implemented, the Dubois model is showing better discrimination between the smooth and rough road regions compared to the other models. But, all the results estimated using the different models need to be validated with respect to the ground truth data. Because so far, although the models provided the surface roughness results with mm as unity, it is not clear whether these estimated "absolute/average roughness" values really represent the true surface roughness and this investigation is currently in progress. Also, further experiments are planned using a new Ka-band sensor which, due to the smaller wavelength, is expected to be much more sensitive to the roughness differences and suitable for detecting smaller cracks and potholes.

References

[1] J. Hofmockel, J. Masino, J. Thumm, E. Sax, and F. Gauterin, "Multiple vehicle fusion for a robust road condition estimation based on vehicle sensors and data mining," *Cogent Eng.*, vol. 5, no. 1, pp. 1–15, 2018.

[2] B. Amini and S. S. Tehrani, "Simultaneous effects of salted water and water flow on asphalt concrete pavement deterioration under freeze-thaw cycles," *Int. J. Pavement Eng.*, vol. 15, no. 5, pp. 383–391, 2014.

[3] B. Mataei, H. Zakeri, M. Zahedi, and F. M. Nejad, "Pavement Friction and Skid Resistance Measurement Methods: A Literature Review," *Open J. Civ. Eng.*, vol. 06, no. 04, pp. 537–565, 2016.

[4] H. Liu, Z. Zhang, D. Guo, L. Peng, Z. Bao, and W. Han, "Research progress on characteristic technique of pavement micro-texture and testing technology of pavement skid resistance at home and abroad," in *2011 International Conference on Remote Sensing, Environment and Transportation Engineering*, 2011, pp. 4368–4372.

[5] K. Laubis, "Crowd-Based Road Surface Monitoring and its Implications on Road Users and Road Authorities," Karlsruhe Institute of Technology, Germany, 2017.

[6] I. H. Woodhouse, *Introduction to microwave remote sensing*. New Delhi, India: CRC Press, Taylor & Fancis Group, 2009.

[7] C. M. H. Unal and L. P. Ligthart, "Decomposition Theorems applied to Random and Stationary Radar Targets," *Prog. Electromagn. Res.*, pp. 45–66, 1998.

[8] E. Pottier, J.-S. Lee, and L. Ferro-Famil, "Advanced Concepts in Polarimetry – Part 1," vol. 2, no. October, pp. 21–22, 2004.

[9] I. Hajnsek, "Inversion of Surface Parameters Using Polarimetric SAR," Friedrich Schiller University Jena, 2001.

[10] J. A. Richards, *Remote Sensing with Imaging Radar*. Springer International Publishing, 2009.

[11] P. Marzahn and R. Ludwig, "On the derivation of soil surface roughness from multi parametric PolSAR data and its potential for hydrological modeling," *Hydrol. Earth Syst. Sci.*, pp. 381–394, 2009.

[12] T. Jagdhuber, "Soil Parameter Retrieval under Vegetation Cover Using SAR Polarimetry," University of Potsdam, 2012.

[13] Y. Oh, K. Sarabandi, and F. T. Ulaby, "An empirical model and an inversion technique for radar scattering from bare soil surfaces," *IEEE Trans. Geosci. Remote Sens.*, vol. 30, no. 2, pp. 370–381, Mar. 1992.

[14] Yisok Oh, "Quantitative retrieval of soil moisture content and surface roughness from multipolarized radar observations of bare soil surfaces," *IEEE Trans. Geosci. Remote Sens.*, vol. 42, no. 3, pp. 596–601, Mar. 2004.

[15] P. C. Dubois, J. van Zyl, and T. Engman, "Measuring soil moisture with imaging radars," *IEEE Trans. Geosci. Remote Sens.*, vol. 33, no. 4, pp. 915–926, Jul. 1995.

[16] M. Keller, J. Fischer, and M. Jager, "F-SAR Product Description," Microwaves and Radar Institute, German Aerospace Center (DLR), Oberpfaffenhofen, 2016.